JUSTUS-LIEBIG-UNIVERSITÄT GIESSEN

Effect of increasing atmospheric CO_2 concentration on vegetation's energy and water limitation

Bachelor Thesis

to obtain the academic degree: Bachelor of Science (B.Sc.) in Environmental Management at the Justus-Liebig-University of Gießen, Germany

presented by:

Marisa Estela Vivanco Sawall

Advisors:

First examiner: Prof. Dr. Lutz Breuer (JLU, Gießen)
Second examiner: Dr. Philipp Kraft (JLU, Gießen)
Dr. René Orth (MPI for Biogeochemistry, Jena)
Chunhui Zhan (MPI for Biogeochemistry, Jena)

marisa.e.vivanco-sawall@en.uni-giessen.de
Matrikelnummer: 6045397

September 30, 2022

Eigenständigkeitserklärung

Ich versichere, dass ich die vorliegende Arbeit selbstständig verfasst und keine anderen als die angegebenen Quellen und Hilfsmittel verwendet habe. Alle Ausführungen, die anderen Schriften wörtlich oder sinngemäß entnommen wurden, sind kenntlich gemacht. Ich habe die Arbeit in gleicher oder ähnlicher Form noch keiner anderen Prüfungsbehörde vorgelegt. Ich stimme zu, dass die vorliegende Arbeit mit einer Anti-Plagiatssoftware überprüft werden darf.

Bietigheim-Bissingen, 30. September 2022.

Marisa Estela Vivanco Sawall

Content

List of Figures

List of Tables

List of Abbreviations

Δ ELI	= difference between ELI calculated for both simulations ($\Delta ELI = ELI_t - ELI_c$)
BNE	= Boreal needleleaf evergreen
BNS	= Boreal needleleaf summergreen
e.g.	= exempli gratia
EF	= evaporative fraction
ELI	= Ecosystem Limitation Index
ELI_c	= ELI calculated with constant CO_2
ELI_t	= ELI calculated with transient CO_2
ELI_{ET}	= ELI calculated with Evapotranspiration anomalies
ELI_{Tr}	= ELI calculated with Transpiration anomalies
Eqn.	= Equation
ET‘	= Evapotranspiration
Fig.	= Figure
GPP	= gross primary productivity
LAI	= leaf area index
LUE	= light use efficiency (GPP/ absorbed photosynthetically active radiation (APAR))
norm_Tr‘	= normalized Transpiration (Tr/LAI) anomalies
rubisco	= Ribulose-1,5-bisphosphate carboxylase/oxygenase
sm‘	= root zone soil moisture anomalies
SWR	= short wave radiation
T	= mean air Temperature
Tab.	= Table
TeBE	= Temperate broadleaf evergreen
TeBS	= Temperate broadleaf summergreen
TeH	= C3 grass
Tr‘	= anomalies for Transpiration of plants
TrBE	= Tropical broadleaf evergreen
TrBR	= Tropical broadleaf rain deciduous
TrH	= C4 grass
VPD	= vapour-pressure deficit

WUE	= water use efficiency

Abstract

Increasing atmospheric CO_2 concentration cause rising Temperature. This are well documented changes in the global environment and its origin in human action is clear (IPCC, 2001a). Forecasting how increasing CO_2 will affect the ecosystem in the future has been the subject of many modeling exercises [Norby and Luo, 2004]. In this study the effect of increasing atmospheric CO_2 concentration on vegetation's energy and water limitation is evaluated with data from the terrestrial biosphere model QUINCY. The Ecosystem Limitation Index is used in this study [ELI; Denissen et al., 2022b] to distinguish between water-energy controlled regimes. It is an Index based on the difference between two correlations, the energy availability correlation reflected by the correlation between Temperature anomalies or short-wave radiation anomalies and Transpiration anomalies, and the water availability correlation represented by the correlation of soil moisture anomalies and Transpiration anomalies [Denissen et al., 2022b]. The study aims to detect if the vegetation is water-controlled or energy controlled to understand if the regime is vulnerable to drought (water-controlled regimes), or benefit from global warming (energy-controlled regimes) [Shakeel et al., 2011, Kumar et al., 2016]. This study shows a shift in time and space towards a more energy-controlled regime. Mainly reflected due to a decreasing correlation between transpiration anomalies and soil moisture anomalies but also the increasing correlation with Temperature or shortwave radiation anomalies plays a role.

Zusammenfassung

Die zunehmende CO_2-Konzentration in der Atmosphäre verursacht einen Temperaturanstieg. Dies sind gut dokumentierte Veränderungen der globalen Umwelt, ihr Ursprung im menschlichen Handeln ist unumstritten (IPCC, 2001a). Die Vorhersage, wie sich die zunehmende CO_2-Konzentration in Zukunft auf das Ökosystem auswirken wird, war Gegenstand vieler Modellierungsarbeiten [Norby und Luo, 2004]. In dieser Studie wird die Auswirkung einer steigenden atmosphärischen CO_2-Konzentration auf die Energie- und Wasserlimitierung der Vegetation mit Grundlage der Daten aus dem terrestrischen Biosphärenmodell QUINCY quantifiziert. Es wird der „Ecosystem Limitation Index" [ELI; Denissen et al., 2022b] verwendet, um zwischen wasser- und energielimitierten Regimen zu unterscheiden. Es handelt sich um einen Index, der auf der Differenz zwischen zwei Korrelationen beruht: der Korrelation der Energieverfügbarkeit, die durch die Korrelation zwischen Temperaturanomalien oder Anomalien der kurzwelligen Strahlung und Transpirationsanomalien widergespiegelt wird, und der Korrelation der Wasserverfügbarkeit, die durch die Korrelation von Bodenfeuchtigkeitsanomalien und Transpirationsanomalien dargestellt wird. Ziel der Studie ist es, festzustellen, ob die Vegetation wasser- oder energiegesteuert ist, um zu verstehen, ob das Regime anfällig für Trockenheit ist (wasserlimitierte Regime) oder von der globalen Erwärmung profitiert (energielimitierte Regime) [Shakeel et al., 2011, Kumar et al., 2016]. Diese Studie zeigt eine zeitliche und räumliche Verschiebung hin zu einem stärker energielimitierten Regime. Dies spiegelt sich vor allem in einer abnehmenden Korrelation zwischen Bodenfeuchtigkeitsanomalien und Transpirationsanomalien wider, aber auch die zunehmende Korrelation mit und Temperatur- oder Kurzwellenstrahlungsanomalien spielen eine Rolle.

1 Introduction

1.1 water- and energy-controlled regimes

In this study water- and energy-controlled regimes are distinguished to detect the influence of increasing CO_2 on them. In the following I want to clarify what characterize water and energy control and how these regimes shift due to increasing soil moisture and increasing evaporative fraction (EF). Water-and energy-control and water-and energy-limitation are used as synonyms in this study.

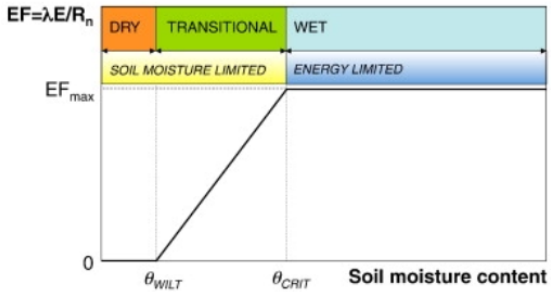

Figure 1. Parameter of energy- and water-controlled regimes [Denissen et al., 2022b].

Fig. 1 distinguish soil moisture-limited (water-limited) and energy-limited regimes. Water-limited regimes are characterized by Evapotranspiration and EF limited due soil moisture [cf. Zhou, 2021]. For energy-limited regimes EF is at its maximum capacity (EFmax). Dry regimes are typical characterized for sites where soil moisture is below the wiliting point (θwilt), here the soil is too dry to extract moisture for Evapotranspiration. After this point water can be extracted from soil. The critical soil moisture (θcrit) shows the transition between water- controlled and energy-controlled conditions. EF increase with increasing soil moisture until the θcrit. Increases of soil moisture after θcrit affect EF no longer [Denissen et al., 2022b].

Now the role of soil moisture and EF for energy- and water-control is clarified. In the following the areas are determine for which these conditions could be applied. Water-limited conditions are found in sites where plenty energy is available. These includes areas with high solar radiation due to rare cloud cover resulting in rare precipitation [Denissen et al., 2022b]. Energy-limited conditions are fulfilled where lot of water is available. Limiting factors for Evapotranspiration are cold temperatures or frequent cloud cover [Denissen et al., 2022b]. Changes between both regimes can be seasonal e.g., due to the strong seasonal cycle of incoming radiation in the mid and high latitudes or due to water availability due to rain seasons in the tropics but weather and climate extremes can also lead to the changes [Denissen et al., 2022b]. Wet periods could shift water-limited regions into energy limitation temporally. Through droughts energy-

limited sites could get water limited due to missing rainfalls and a resulting clear sky (Hauser et al., 2016).

It's important to know if the vegetation is energy or water-controlled because ecosystem responses depend on that [Denissen et al., 2022a]. If they are water-controlled, they are vulnerable to drought but not much affected by changes in temperature or radiation [Shakeel et al., 2011]. If they are energy-controlled they are not much affected by deficits in precipitation or soil moisture but might be able to benefit from global warming (if they stay energy-controlled over the next decades) [Kumar et al., 2016].

Rising temperatures due to global warming in recent years and beyond are affecting plant physiology e.g., the photosynthesis [Hughes, 2000]. Temperature increases could benefit photosynthesis if the vegetation is energy-controlled through the RubisCO (Ribulose-1,5-bisphosphate carboxylase/oxygenase) enzyme which controls the rate of photosynthesis or carbon assimilation – resulting in a positive effect on photosynthesis [Sage et al., 2008]. With increasing temperature VPD (Vapour-pressure deficit) increases in water-controlled regimes. VPD reflect the strength of moisture sucked out of soil and plants. The result of the increasing VPD is an increase of the soil moisture deficit and a stronger water limitation – resulting in a negative effect on photosynthesis [Prenger and Ling, 2001]. In the case of temperature increasing both processes, rubisco and VPD, operate in both energy- and water-controlled conditions, but in energy-limitation the rubisco response is dominant and in water-controlled conditions the VPD response is dominant. This is an example why it is important to know about water- vs energy-controlled conditions as they affect which processes matter for photosynthesis [cf. Lawlor, 2002, Wilhelm and Selmar, 2011]. To also consider the effect of increasing CO_2 for these mechanisms, VPD rise with increasing CO_2 parallel to the increasing Temperature (hotter and dryer climate conditions causes increasing CO_2). The productivity of the vegetation is negatively impacted due to the rising atmospheric demand this could be compensate due to the positive effect of CO_2 fertilization for the vegetation [Kolby et al., 2016]. The CO_2 fertilization effect is the increased vegetation productivity due to increasing CO_2 concentration [Wang et al., 2020]. The CO_2 fertilization is also directly coupled with the Rubisco enzyme. The leave level effect of the fertilization directly includes the biochemical effect of increasing CO_2 for the Rubisco activity. Terrestrial plants shown a natural ability to adapt this effect of increasing CO_2 [Tommasi, 2021], more information about the effects of increasing CO_2 in section 1.3.

The described mechanisms (e.g., rubisco, stomatal conductance) are dependent on energy- vs. water-controlled conditions but this can be different depending on vegetation types. This means that the same soil moisture, Temperature and radiation conditions could lead to energy-

controlled conditions for some plants, including the respective responses of their rubisco and stomata conductance, while for other plants in the same area it can lead to water-controlled conditions [Cao et al., 2017, Medlyn et al., 2001]. To summarize this, with changing soil moisture and Temperature the fraction of water-controlled vs. energy-controlled plants change, and the degree of their water- vs. energy-control.

1.2 Introduction of ELI

In this study an index is used to get to know if the vegetation is water-controlled or energy-controlled, the Ecosystem Limitation Index (ELI; Denissen et al., 2022b). The index includes information about the water availability through soil moisture (sm'). Sm' influence land-atmosphere interactions and is used as the hydrologic variable regulating net ecosystem exchange [Ochsner et al., 2013]. The ELI includes information about the energy availability through temperature (T') or shortwave radiation (SWR'). SWR' reflects one part of the radiant energy incident, the radiation on 280 to 2800 nm on a horizontal surface from all directions [Klassen and Bugbee, 2005]. In any case radiation is the only source of energy for photosynthesis, while T' affects the activity of the rubisco enzyme and hence how fast assimilated carbon can be processed by plants, so in the end both energy variables are relevant through different physical pathways [Dogutan and Nocera, 2019, Sage et al., 2008].

The ELI is computed by the difference between two correlations, the correlation between anomalies of soil moisture (sm') and transpiration (Tr') and the correlation between anomalies of T' or SWR' and Tr' (cf. Equ. (1)). The single quotation marks denote the detrended and deseasonalized values of the variables.

$$ELI = cor\,(sm', Tr') - cor\,(T'\ or\ SWR', Tr') \qquad (1)$$

With ELI = Ecosystem Limitation Index, sm' = soil moisture [m], T'= Temperature [K], SWR' = short wave radiation [w m^{-2}] and Tr' = Transpiration [kg m^{-2} day^{-1}].

The value of the result gives us information about the region if it's energy- or water-controlled. If the ELI is higher than zero, the region is water-controlled. With a result below zero the region is energy-controlled [Denissen et al., 2022b].

1.3 What do we expect the ELI to change with increasing CO2?

In Fig. 2 the effects of increasing CO_2 for plants are shown.

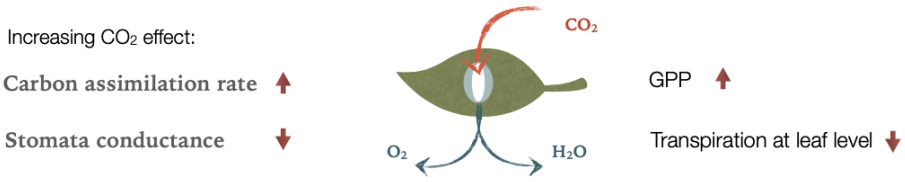

Figure 2. Effect of increasing CO2 for plants.

Increasing CO_2 leads to changes in atmospheric conditions which results in an increased plant productivity [Zhan et al., 2022]. The increase of CO_2 stimulates the carbon assimilation and reduces the stomatal conductance [Ainsworth and Long, 2005]. A consequence of this is the increase of light-use efficiency (LUE) and water-use efficiency (WUE) of plants and thus less water limitation [Ueyama, 2020]. Both effects result summarized in the CO_2 fertilization effect. This effect leads to changes in gross primary productivity (GPP) and transpiration that result in changes for the carbon and water cycles [Walker et al., 2021]. The changes of GPP results in changes in the net primary production (NPP) which leads to an increased biomass production. This is seen in an increasing leaf area index (LAI). Increasing CO_2 change transpiration and other components of the water cycle [Lemordant et al., 2018]. The following effects of increasing CO_2 are competing [Zhan et at., 2022]. The reduced Transpiration at a leaf level is due to the decreased stomatal conductance [Ainsworth and Roger, 2007] which results in less water limitation with increasing CO_2. This can be compensated by an increase in the leaf area and thus Transpiration at canopy level at the same time because more carbon is needed for the leaf growth [Wullschleger et al., 2002]. This can result in a non-detectable effect for the water cycle [Zhan et al., 2022].

To calculate the ELI a model (more information in 2.1) was used because this way we can compare how plants and ecosystems respond to changes in CO_2 exclusively, while in the real-world changes in are happening at the same time as changes in climate, such that the observations only show the combined effect. It remains unclear how much of this is related to CO_2 and how much is related to climate changes [Norby and Luo, 2004].

This study aims to understand how an increase of CO_2 affects the energy and water limitation of vegetation. For this study we test the hypothesis if the vegetation gets less water controlled at leaf level with increasing CO_2.

2 Material and methods

2.1 Data and simulation

The data I use for this study is calculated with the terrestrial biosphere model QUINCY (Quantifying Interactions between terrestrial Nutrient CYcles and the climate system; Thum et al., 2019). QUINCY represents for terrestrial ecosystems the coupled carbon, nitrogen and phosphorus cycles and their interactions with water and energy balances across the water- and energy-controlled regimes and different plant function types (PFTs; Tab. 1) [Zhan et al., 2022]. I imitate the observational setting in ecosystem by using this process-based land surface model to study the leaf-level effects of increasing CO_2 [Zhan et al., 2022]. There are differences with studying the effect of increasing CO_2 for the ELI at leaf and ecosystem level. At leaf level increased CO_2 leads to higher water use efficiency. At ecosystem level the plant benefits from the higher leaf-level water use efficiency and grows more leaves such that the water loss increases again which limits the increase in water-use efficiency (cf. 1.3). The calculations and analyses in this work are based on the data of 118 years in the period from 1990 to 2018. I use daily data for every variable for these 118 years. The data for this study cover 336 sites distributed all along the globe. The calculations and analyses were generated by Python 3.6.13 with Visual Studio Code. I use the packages numpy and pandas to compute the calculations. To create plots I use the package matplotlib.pyplot. I prepare the global maps with the packages cartopy and seaborn.

Table 1. Vegetation classes and PFTs used in this study.

Vegetation classes	PFT defined in the QUINCY model
Tropical Forest	Tropical broadleaf evergreen (TrBE)
	Tropical broadleaf rain deciduous (TrBR)
Temperate Forest	Temperate broadleaf evergreen (TeBE)
	Temperate broadleaf summergreen (TeBS)
Boreal Forest	Boreal needleleaf evergreen (BNE)
	Boreal needleleaf summergreen (BNS)
Grass	C3 grass (TeH)
	C4 grass (TrH)

The sites we analyse in this study can be summarized in four vegetation classes. Every vegetation class includes two Plant functional types (PFTs). PFTs contain a classification scheme which represent species and broad vegetation types (Duckwoth et al., 2000). They are derived from characteristics based on species morphology, physiology and/or life history (Ustin and Gamon, 2010).

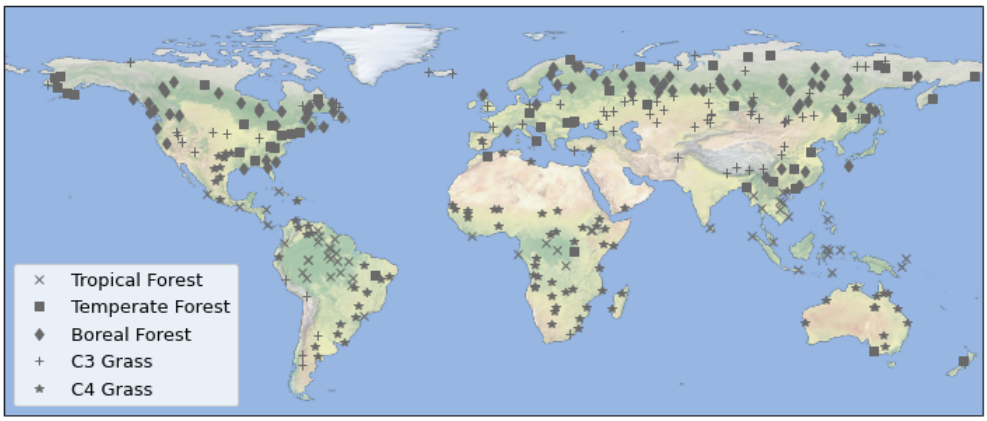

Figure 3. Spatial distribution of vegetation classes.

Fig. 3 shows the distribution of the measuring points globally. The legend represents the vegetation classes used in this study (Tab.1). The Tropical Forests are distributed in the southern hemisphere, more precisely in regions in south America, central Africa, and south Asia. The Temperate Forest is mostly distributed in the northern hemisphere in north America, Europe and north and central Asia. Temperate Forests are sporadically found in the northern hemisphere as well. Boreal Forests are based in the northern hemisphere, in north America, Europe and in north and central Asia. C3 grass can be found in north and south America, and in Europe and north and central Asia as well. While C4 grass can be found in the south of north and south America, in south Africa and in Australia. I differentiate both types of grass because they have a different response of increasing CO_2. While the photosynthesis in C4 plants is saturated earlier, the C3 plant show stronger increase in the carbon assimilation rate [Ainsworth and Rogers, 2007]. This means that C3 plants have a higher response to increasing CO_2 associated with a high WUE [Way et al., 2014].

This study is based on two simulations with identical climate but varying CO_2 concentrations. One of the simulations assumes increasing CO_2 (transient CO_2) as observed with an increase of 110.63 ppm until the year 2018. The other simulation assumes constant CO_2 at the level of year 1901 (296.8 ppm)). The different CO_2 concentration results in different sm' and Tr' between the transient- and the constant- CO_2 experiment.

2.2 Overview of analyses

This study includes several analyses. a) The base for this study is the result of the calculation of ELI which tells us if the region is water or energy controlled. b) The differences between the results for ELI when computed with several different components c) I analyse the drivers of the

spatial variability of ELI changes by fitting the sensitivity of ELI to CO_2 with different variables into a linear regression. I quantify these changes by contrasting the vegetation classes. d) The last study is about attribution of ELI changes in time which shows us to what extent structural and physiological changes affect the ELI by calculating partial correlations. The results for the analyses are shown on different time scales. I calculate ELI for all years, for selected dry years and for the month with the highest Transpiration.

2.3 Information about the analyses on site scale

I look at the results on a global view by considering all sites but also select three sites to better understand changes in the ELI.

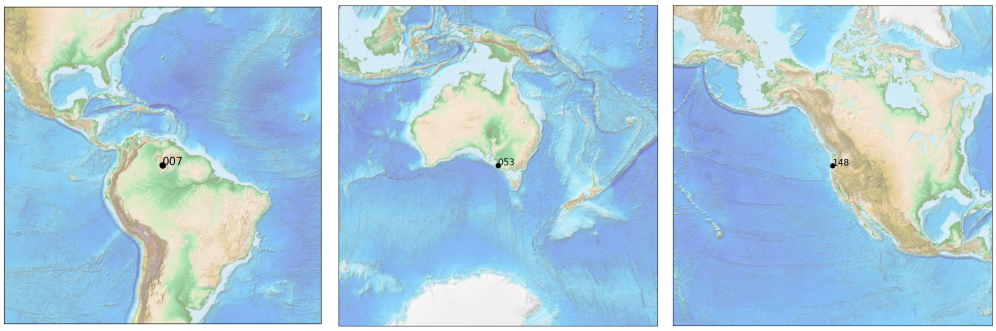

Figure 4. Represented sites for analyses on site base: Tropical Forest, Temperate Forest and Boreal Forest (from left to right).

For the tropical forest I select a tropical broadleaf evergreen in the north of south America. For the Temperate Forest I choose a Temperate broadleaf evergreen in south Australia. The boreal forest is represented by a Boreal needleleaf evergreen on the west coast of the United States (Fig. 4).

2.4 Analyses in this study

2.4.1 a) Calculation of ELI

First, I write a function which read the data from QUINCY and load the file as a data frame. Now I select the target variable from the data frame and generate a time series with start and end date. Afterwards I remove the long-term trend and seasonal cycle of sm', T' and SWR'. For sm' values I use data from soil moisture of the root zone. The data for T' are mean air temperature values. For SWR' I use short-wave radiation. For each site I calculate the correlation between sm' and SWR', and between sm' and T'. If the value for the correlation between sm' and T' is higher than the value for the correlation between sm' and SWR', T' is used to

represent the energy limitation, vice versa. So the highest correlation with sm' is used to represent energy availability for ELI (Fig. 5).

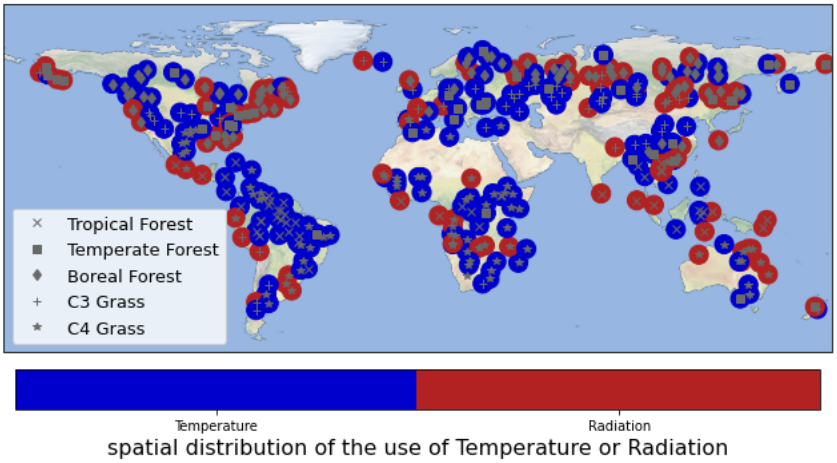

Figure 5. Spatial distribution of the use of temperature or radiation to compute the ELI.

The global map shows the energy variable for every site where I use T' or SWR' (Fig. 5). In south Africa and south America as well as in Europe and some sites in north America and Asia T' is most used. SWR' is used to calculate the ELI in sites in south Asia, high latitude sites in the northern hemisphere and especially sites near to the coast across the globe.

After deciding whether I should use T' or SWR' to calculate the ELI I filter the growing season. I compute the growing season to exclude months when the vegetation is not active given the low temperature. I identify three different filters to create a mask for the variables used in this study.

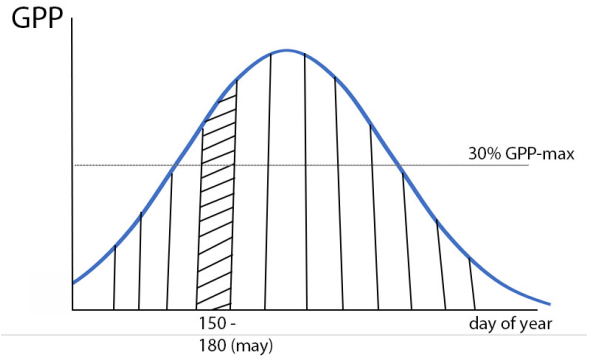

Figure 6. GPP filter for the growing season.

Fig. 6 shows a schematic illustration of how the first filter is computed. The first filter is calculated based on GPP. GPP includes the amount of CO_2 that is that is assimilated by plants through

photosynthesis [Joiner et al., 2018]. At leaf level plants fix CO_2 as organic compounds by net photosynthesis. The gross uptake of CO_2 at ecosystem scale is called GPP [Anav et al., 2015]. The GPP filter includes all the data where GPP is higher than 30 % of the maximum of GPP. The second filter includes all data where Temperature is higher than 5 degrees Celsius. The third filter is to select months where both conditions remain more then 15 days. With 15 days a threshold is set of how many days should be included to add the month into the growing season.

The next step is normalizing transpiration due dividing transpiration by LAI to exclude the potential compensating effect of increasing LAI (cf. 2.1). The LAI (in m^{-2} m^{-2}) quantifies the amount of leaf area in an ecosystem and is therefore a structural vegetation variable that is essential in the feedback of vegetation in the climate system [Fang et al., 2019]. This normalized Tr is used to calculate the water- or energy limitation at leaf level. Next, I remove the long-term trend and seasonal cycle of normalized Tr (norm_Tr'). The norm_Tr' is used by now in all studies to compute the ELI. Finally I calculate the ELI. The calculation of ELI for transient and constant CO_2 is presented in the following Equ. (2) and (3) (cf. general Equ. (1) for ELI). The single quotation marks denote the detrended and deseasonalized values of the variables.

Calculation of the ELI in the transient- CO_2 experiment (ELI_t):

$$ELI_t = cor\left(sm_t' , \frac{Tr_t'}{LAI'}\right) - cor\left(T' or\ SWR', \frac{Tr_t'}{LAI'}\right) \quad (2)$$

with ELI_t = ELI calculated with transient CO_2, sm = soil moisture [m], Tr/LAI = normalized Transpiration [kg m^{-2} day $^{-1}$], T = Temperature [K] and SWR = short wave radiation [w m^{-2}].

Calculation of the ELI in the constant-CO_2 experiment (ELI_c):

$$ELI_c = cor\left(sm_c' , \frac{Tr_c'}{LAI'}\right) - cor\left(T' or\ SWR', \frac{Tr_c'}{LAI'}\right) \quad (3)$$

with ELI_c = ELI calculated with constant CO_2, sm = soil moisture [m], Tr/LAI = normalized Transpiration [kg m^{-2} day^{-1}], T = Temperature [K] and SWR = short wave radiation [w m^{-2}].

To perform the calculation of the ELI I create a data frame and insert the correlation components. Then I group the data by year and calculate Pearson correlations. The Pearson correlation as similarity measures evaluate how much two variables are correlated [Sheugh and Alizadeh, 2015]. After I calculate the difference between both correlations to get ELI_t and ELI_c (cf. Equ. (2) and (3)) I calculate the difference between both simulation (Δ ELI).

$$\Delta ELI = ELI_t - ELI_c \quad (4)$$

With Δ ELI = Difference of ELI, ELI_t = ELI calculated with transient CO_2, ELI_c = ELI with constant CO_2.

This difference (Δ ELI) quantifies the effect of increasing CO_2 on ELI.

Following global maps are created to show the spatial distribution of ELI. These maps are created for the ELI calculated for the month with the highest transpiration. With high transpiration the vegetation is most active and therefore a larger effect of increasing CO_2 for ELI can be detected [Porporato et al., 2001]. Transpiration effecting the ecosystem for example due to surface cooling [Konarska et al., 2016]. A less energy-limited regime is expected when only considering the month with the highest transpiration because of the high atmospheric water demand. This is associated with higher temperatures and therefore Temperature is no longer limiting [Denissen et al., 2022a]. Plants become less energy limited in energy-controlled regions due to the increased LUE (cf. 1.3). Global maps represent the value for every site from the month with the highest Transpiration. For this every month for every site is considered. The components of ELI are grouped by month and the ELI is calculated afterwards. The result shows a list with values for every month in the growing season for every site. Next, I select the month with the highest transient Tr for every site. I get a global list with one value for every site which represents the value of the month with the highest Tr. To plot the global map for ELI calculated with transient and constant CO_2 I calculate the 0,05% and 0,95% quantile for both variables and use these values to create the global maps. The quantiles are used to remove outliers which could distort the distribution of the values.

2.4.2 b) ELI computed with Tr', norm_Tr' or ET'

The water and energy availability components of ELI are reflected due a correlation with norm_Tr' for all our analysis. To see the effect of other factors we also use Tr' and ET' in this analysis. Both variables play an important role in the energy and water balance of the land surface [Pieruschka et al., 2010]. ET' (in kg m^{-2} day^{-1}) includes three components that have different stores of water and different characteristic timescales. Tr' is one of the three components of ET'. The other two are Interception and soil surface evaporation [Blyth and Harding, 2011]. Tr' reflects with 80% amount of total ET' the largest component of ET' [Miralles et al., 2011]. The variable Tr' contains the water loss of plants through the stomatal pores of leaves [Pieruschka et al., 2010]. Norm_Tr' represents Tr' at leaf level (cf. 2.4.1). For this analysis plots are created that reflect Attribution of Δ ELI with changes in space for different sites (Fig. 4;

approach in the following section 2.4.3). The plots include on the x-axis values for the increasing CO_2 and on y-axis the Δ ELI.

2.4.3 c) Attribution of ELI with changes in space

For this analysis Attribution of ELI with changes in space are considered to detect changes of attribution for changes in Δ ELI. The 10 driest and wettest years among the last 20 years are selected based on the absolute soil moisture to distinguish the results for wet and dry site. Plots with CO_2 on the x-axis and Δ ELI on the y-axis reflects the sensitivity of Δ ELI to CO_2 for three sites (Fig. 4). I insert a regression line to detect a trend of changes in Δ ELI with increasing CO_2 and a dashed line parallel to x-axis at the level of ΔELI = 0 to distinguish between energy and water-controlled regimes. Fig. 21 shows the sensitivity of Δ ELI to CO_2 for all sites. The values shown on the maps represents the slope of the regression line between Δ ELI (and its components) and CO_2. The result is a data frame for the ELI in the 10 driest and wettest years and a list as an output with all sites and the values for the sensitivity of ELI. In the next step the main driver for changes in the sensitivity of ELI are detected. To quantify the changes from these variables for changes of the sensitivity Δ ELI to CO_2 Multilinear regressions are used. Multilinear regressions create a linear relationship between two variables – the dependent and independent variable. This results in a prediction of the values for the dependent variables given new values of independent variables [Su et al., 2012]. We use this tool to predict the effect of different driver for changes in the sensitivity of Δ ELI to CO_2. I fit two linear regression models for dry years and wet years separately. I evaluate the contribution of Temperature, LAI, canopy height and aridity to the sensitivity of Δ ELI to CO_2. These variables change spatially and thus reflect spatial changes for Δ ELI. The aridity is reflected due to the Bowen ratio. It's the ratio of the sensible heat flux to latent heat flux and impact the warming extent of available energy to the ecosystem land surface air [Tang et al., 2014]. I distinguish the effect from the parameters for different PFT by making linear regression for every PFT. To calculate the linear regression the target variable, the sensitivity of Δ ELI are first defined and the input variables (Temperature, aridity, height, LAI) were loaded. All the input and target variables are normalized so that the range of each variable is from 0 to 1. After this I merge all normalized variables in one data frame and calculate the Multilinear regression. Further I get variables for the influence of every variable for the target variable and a p-value for this influence. The higher the resulting absolute variable the greater the influence for the target variable.

2.4.4 d) Attribution of ELI with changes in time

To calculate attributions of ELI with changes in time the variables Δ LAI, Δ Tr/LAI and Δ GPP/APAR are selected. Delta (Δ) reflects the difference of the variable calculated with transient and constant CO_2 (similar calculation as in Equ. (4)). Δ GPP/APAR reflects the light use efficiency of photosynthesis which reflects the efficiency of energy transformation for CO_2 assimilation (LUE; cf. 1.3) [Yang et al., 2018]. To reduce high fluctuation of the variable during the years and detect a clear trend of changes for ELI we use sliding windows. With sliding windows calculation are computed for every consecutive 10 years (e.g., 1901-1910, 1902-1911). I define the window size by 10 years. For this an empty list to store moving averages that consider every window size of 10 years must be initialize. The average of the current window must be calculated, and the stored for the current window in the moving average list. At least the window should shift right by one position.

Now I calculate the difference (Δ) of the value for the variables calculated for transient CO_2 and constant CO_2. Plots demonstrate the changes for Δ LAI, Δ Tr/LAI and Δ GPP/APAR over time (Fig. 24-26). The x-axis reflects the timeline with sliding windows on the y-axis the values of the tested variable are represented. Next, I calculate the ELI also with sliding windows. I keep the window size by 10 years. An empty list is created to store the moving correlation for every window size of 10 years and the correlations are calculated to compute the ELI. Then I group the ELI by year. After that I store the average of the current window in the moving average list and shift the window right by one position. To understand the effect of changes in structural and physiological variables for changes in Δ ELI I calculated partial correlations. Partial correlations are used to quantify the correlation between two variables when several variables are conditioned [De La Fuente et al., 2004]. As a proxy for structural changes, we use Δ LAI. For physiological changes Δ Tr/LAI and Δ GPP/APAR (LUE) have been used (cf. 1.3). Three partial correlations for the different driver are initialized. The x-value denotes the input variable whose influence want to be evaluate. The y-axis reflects the constant variable Δ ELI which influencing changing effects we want to quantify. The first partial correlation calculates the effect of Δ Tr/LAI to Δ ELI by considering the effect of Δ GPP/APAR and Δ LAI as third variables. Therefore, confounding factors (Δ LAI, Δ GPP/APAR) are excluded to detect physiological changes from Δ Tr/LAI. The second correlation detect the influence of Δ LAI to Δ ELI by including the third variable Δ GPP/APAR and Δ Tr/LAI. And the third correlation includes the influence of Δ GPP/APAR for Δ ELI by consider Δ Tr/LAI and Δ LAI as third variables. By determine third variables the collinearity for the correlation between ΔELI and the input variables is removed. The method I use to calculate these three calculations are spearman

correlations. Spearman correlations measures the strength of a relationship between two variables [Hauke & Kossowski, 2011]. The results for the partial correlation are round by three numbers. A value for the spearman correlation and a p-value for the calculation are the result for this analysis.

3 Results

3.1 Results for the analyses

The single quotation marks in the following section denote the detrended and deseasonalized values of the variables.

3.1.1 a) Calculation of ELI

The following section takes a closer look at the ELI and its components. Values for all 118 years are considered in the results on site scale.

Table 2. Relationship of ELI and its components to water and energy limitation [Denissen et al., 2022b].
Cor = Correlation, ET = Evapotranspiration [kg m^{-2} day^{-1}], sm = soil moisture [m], T = Temperature [K], SWR = short wave radiation [w m^{-2}], ELI = Ecosystem Limitation Index

Regime	Water limitation	Energy limitation
Cor(sm', ET')	> 0	< 0 or ≈ 0
Cor(T' or SWR', ET')	< 0 or ≈ 0	> 0
ELI	> 0	< 0

In Tab. 2 the values for ELI and its component and how they differ between water and energy limited regimes is represented.

In the following the results for the three selected sites (Fig. 4) are shown to detect changes over time and see different results for different vegetation types. The absolute ELI (ELI calculated with constant and transient CO_2) and its components are shown.

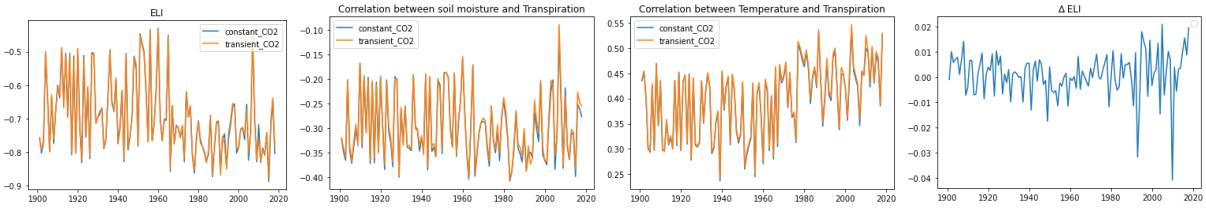

Figure 7. Time series of ELI from transient-CO_2 and constant-CO_2 experiments their components and Δ ELI for the Tropical Forest.

The ELI calculated with transient and constant CO_2 shows an energy-controlled regime over the entire time period for the tropical forest. With negative values for the correlation of sm' and

norm_Tr' and positive values for the correlation of T' and norm_Tr' the ELI get negative values (Tab. 1). Δ ELI show shifts between the water-controlled and the energy-controlled regime for some years.

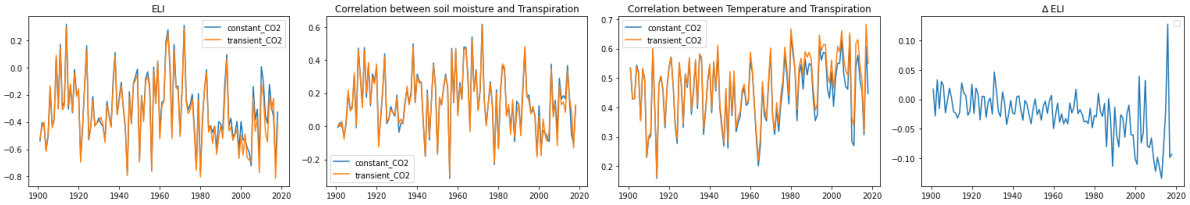

Figure 8. Time series of ELI from transient-CO_2 and constant-CO_2 experiments their components and Δ ELI for the Temperate Forest.

Most of the years the regime is under energy-control for the absolute ELI in the Temperate Forest. For some years, especially in the first 80 years the regime is water-controlled. There are some differences for the last 40 years between both calculations (ELI_t and ELI_c). Both components of the ELI are positive for all the years while there is an increase of the T' Correlation calculated with transient CO_2 for the last 60 years. Δ ELI shows a decreasing trend towards a strong energy-controlled regime.

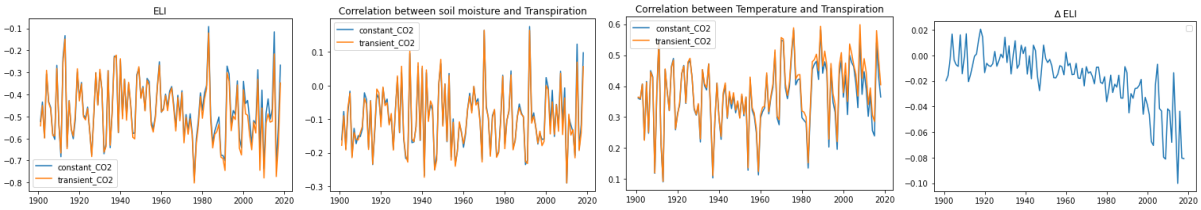

Figure 9. Time series of ELI from transient-CO_2 and constant-CO_2 experiments their components and Δ ELI for the Boreal Forest.

Figure 9. Time series of ELI from transient-CO_2 and constant-CO_2 experiments their components and Δ ELI for the Boreal Forest.

The Boreal Forest is energy controlled with a stronger energy control for ELI_c for the last 40 years. With positive values for the correlation with radiation and values near to zero for the Correlation with sm the ELI gets negative (Tab. 1). For Δ ELI there is a strong decrease over time.

To get an idea for the spatial distribution of the ELI I plot the ELI calculated with both simulations, their difference (Δ ELI) and the components of Δ ELI for the month with the highest transpiration on a global scale. With the global maps you can see the spatial pattern of high and

low values. In general, are sites located in the north and the south (tropics) strongly energy controlled. In Europe most of the sites are less energy controlled.

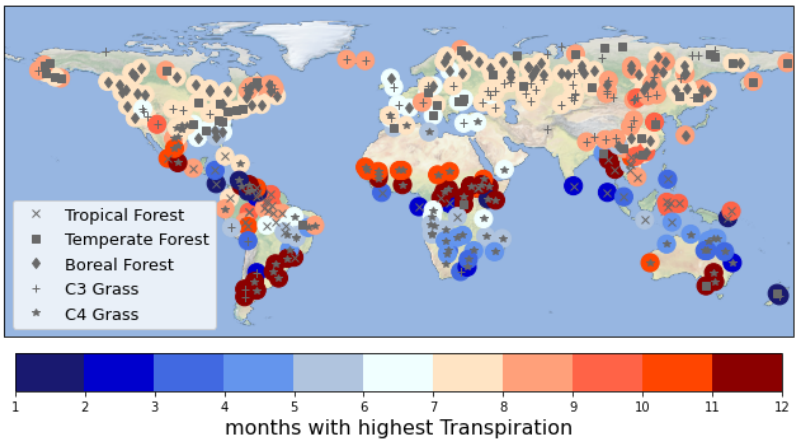

Figure 10. Global map for the months with the highest transpiration.

Fig. 10 shows a global overview of the months with the highest transpiration. There are major differences for the calculated month between the northern and southern hemisphere. In the norther hemisphere the month with the highest transpiration is in the summer between July and September. Near the equator the month with highest transpiration occur between August and November while in the southern hemisphere it's between December to May. A globally decreasing spatial trend from the northern to the southern hemisphere are detectable from warm to cold months.

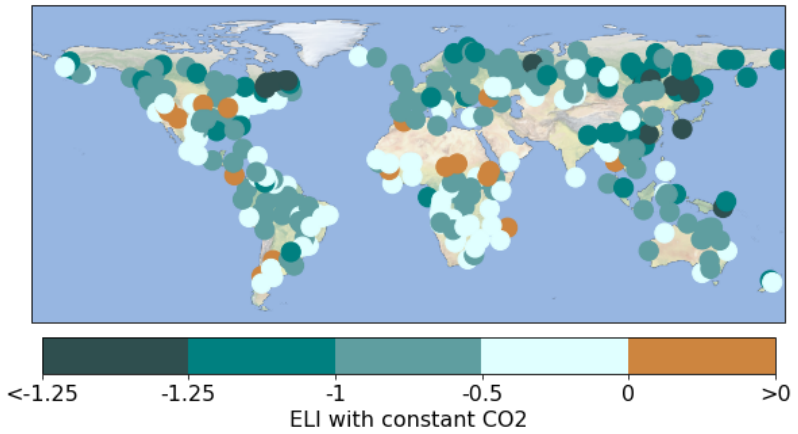

Figure 11. Global map for the ELI calculated with constant CO_2.

Most of the sites are energy-controlled (ELI < 0) with constant CO_2. Only some sites in Africa, north and south America and sporadically in other regions are slightly water-controlled (Fig. 11).

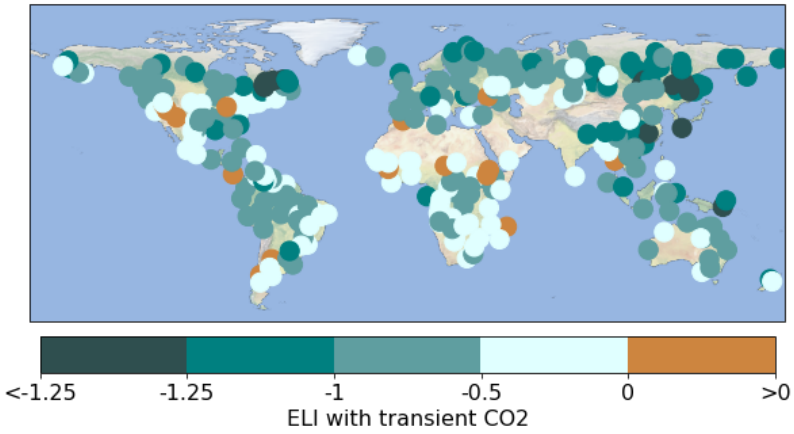

Figure 12. Global map for the ELI calculated with transient CO_2.

There is no clear difference with increasing CO_2 detectable (Fig. 12).

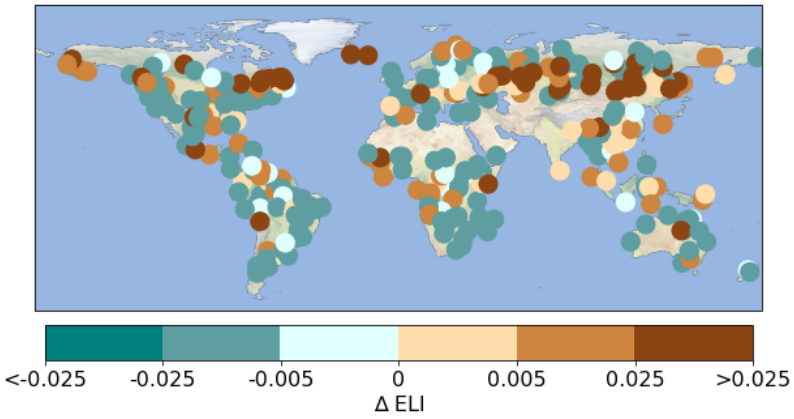

Figure 13. Global map for the Δ ELI.

In Fig. 13 the global ecosystem is generally under widespread energy control. Δ ELI shows that high latitude sites in the northern hemisphere are getting less energy controlled. For other sites, ecosystem is getting more energy controlled, or in another word, getting less water controlled.

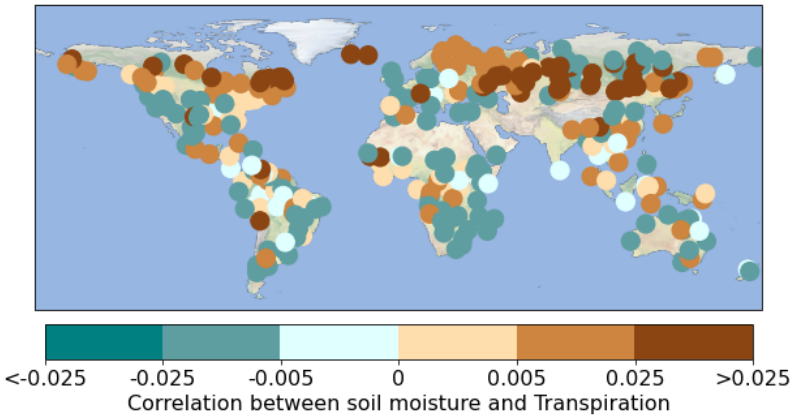

Figure 14. Global map for Δcor (sm',Tr_norm').

To understand what influences the Δ ELI (Fig. 13) most, we look at each component of the Δ ELI in detail (Δcor (sm',Tr_norm') and Δcor (T' or SWR' ,Tr_norm'). They denote the difference for water and energy availability for the transient and constant CO_2 scenarios. In Fig. 14 the Correlation which reflects the water availability of ELI is shown. The correlation of Δ sm' and Δ norm_Tr' influence Δ ELI the most. Positive correlations are mainly distributed in high latitude sites in the northern hemisphere e.g., in Russia and Canada. Positive correlations are also detected in north of south America, mid of Africa and Indonesia. Negative correlation can be seen in Europe, north and south America, main parts of Africa, Australia, and the USA.

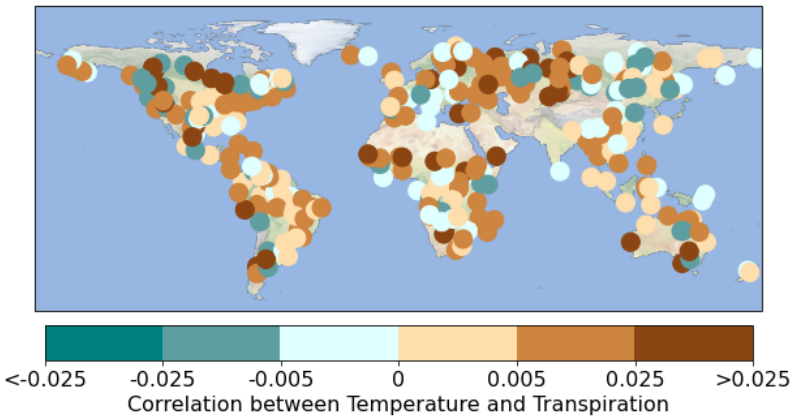

Figure 15. Global map for Δcor (T' or SWR',Tr_norm').

In Fig. 15 most of the sites have positive correlation between Δ T' and Δ Tr_norm'. High values cumulate especially in south America, south Africa, Europe, and Canada. Only some sites in North America and Asia have slightly negative values for the component of ELI which reflects energy availability.

3.1.2 b) ELI computed with Tr, Tr/LAI or ET

For analysis b) and c) I will show plots and maps for the calculation with the 10 driest years.I chose the 10 driest year to see a stronger effect of CO_2 to Δ ELI.

In this analysis we compute Δ ELI with different variables we use norm_Tr' (ELI) – the variable we use in all the other analyses – and we use Tr' (ELI_{Tr}) and ET' (ELI_{ET}) to see how results change. To identify these changes, we use one of selected sites, the Boreal Forest (Fig. 4) and look at the results for the sensitivity of Δ ELI to CO_2 calculated for the 10 driest years (cf. Equ. (4)).

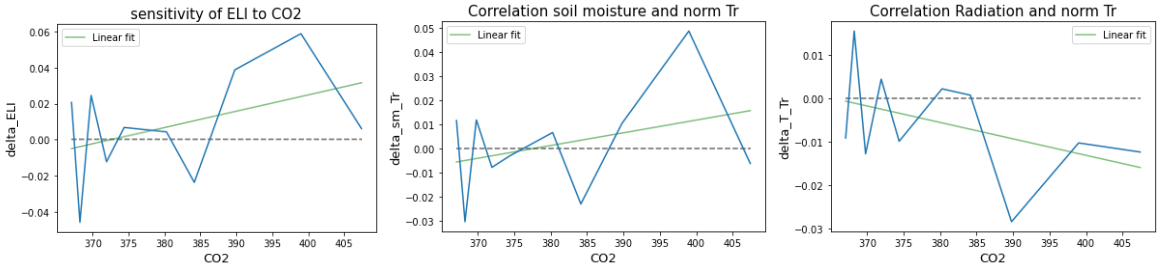

Figure 16. Sensitivity of Δ ELI and its components to CO_2 with norm_Tr'.

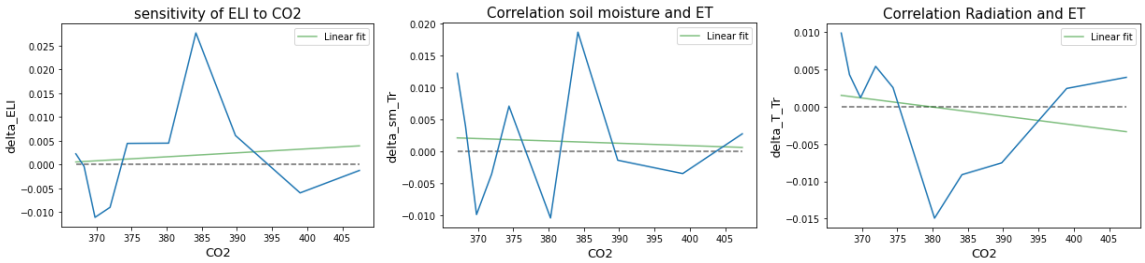

Figure 17. Sensitivity of Δ ELI and its components to CO_2 with ET'.

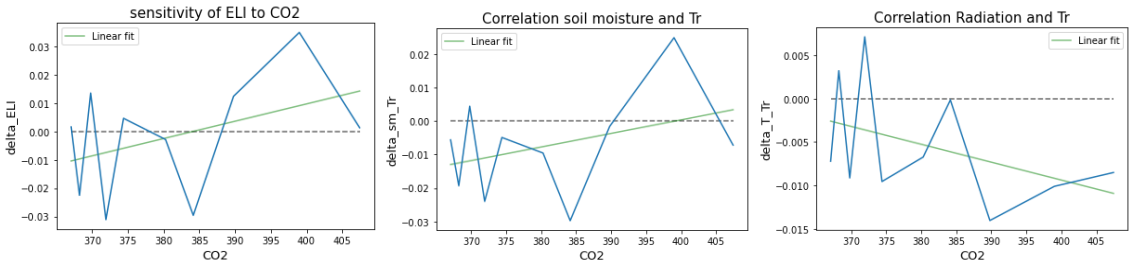

Figure 18. Sensitivity of Δ ELI and its components to CO_2 with Tr'.

With increasing CO_2 the Boreal Forest shift from an energy-controlled regime to a water-controlled regime. Clear differences for the results when we compute Δ ELI with different variables are detectable. These changes happen on different CO_2 levels. The ELI and ELI_{ET} shifts earlier from an energy-controlled regime to a water-controlled regime (370-375 ppm) than ELI_{Tr} (385 ppm). With a high CO_2 concentration in the atmosphere (405 ppm) ELI gets water-controlled

the most followed by ELI_{Tr}. With ELI_{ET} we can hardly see any changes between the energy and water-controlled regimes. When we look at trends of the components of ELI calculated with Tr', ET' and norm_Tr' we even see different trends for the Correlations. The Correlation of sm' with Tr' results in an increase of ELI and ELI_{Tr} with increasing CO_2 while the Correlation for ELI_{ET} tends to gets slightly more negative. For Δ ELI we have similar trend towards negative values with increasing CO_2. ELI and ELI_{Tr} get strongly negative while there are hardly differences of ELI_{ET}.

3.1.3 c) Attribution of ELI with changes in space

In the following study the sensitivity of Δ ELI and its components is quantified. Two Figures with the results for the other selected sites – the Tropical Forest and the Temperate Forest (Fig. 4) are shown calculated with norm_Tr'.

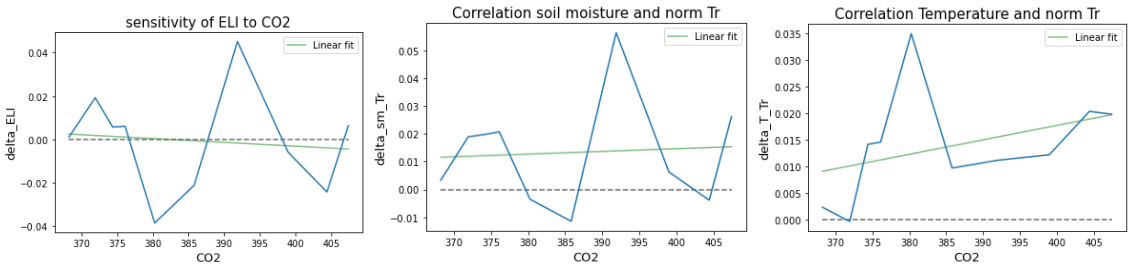

Figure 19. Sensitivity of Δ ELI and its components to CO_2 in the Tropical Forest.

The first site we want to have a look is the Tropical Forest. There is a weak decrease of Δ ELI with increasing CO_2. With more than 385 ppm the Tropical Forest shift from slightly water-controlled to a slightly energy-controlled regime. With a correlation of sm' and norm_Tr' near to zero and a positive correlation between T' and norm_Tr' the ELI gets negative, and the region is energy-controlled (Tab. 1).

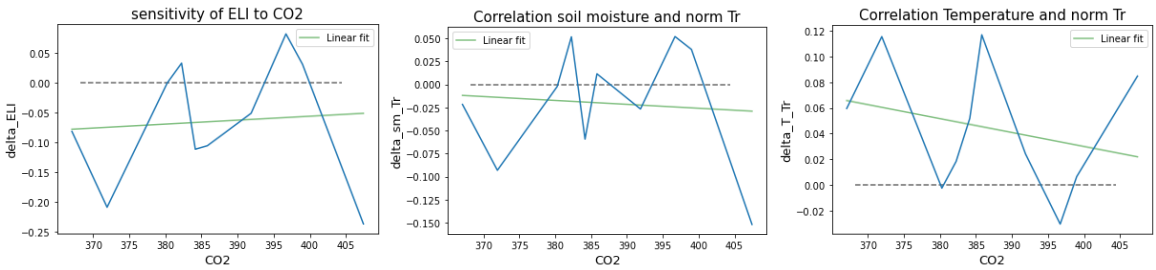

Figure 20. Sensitivity of Δ ELI and its components to CO_2 in the Temperate Forest.

This Temperate Forest is an energy-controlled regime. It gets slightly more water limited or in other words less energy controlled with increasing CO_2. With a negative correlation of sm' and norm_Tr' near to zero and positive Correlation of T' and norm_Tr' the variables for Δ ELI get negative, indeed energy control (Tab. 1).

For the sensitivity of Δ ELI and its components to CO_2 for the Boreal Forest (Fig. 16) there is a shift from energy-controlled to water-controlled regimes on a CO_2 level of ~375 ppm. With a positive Correlation for sm' and norm_Tr' and a negative Correlation between SWR' and norm_Tr' the calculated values for Δ ELI are positive (Tab. 1).

For all sites there are many fluctuations for Δ ELI with increasing CO_2. The linear regressions line tries to show a trend between all the fluctuations.
In the following the spatial distribution over the globe for the sensitivity of Δ ELI to CO_2 within the 10 driest years are shown.

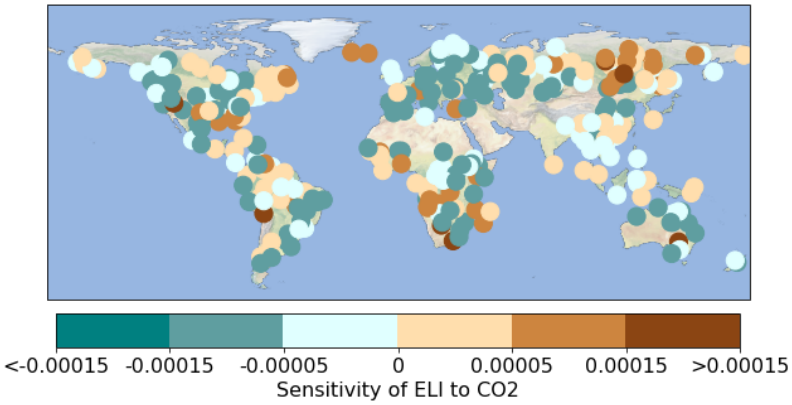

Figure 21. Global map for the sensitivity of Δ ELI to CO_2.

Globally most sites are energy-controlled for the sensitivity of Δ ELI to CO_2 especially in Europe. Some regions in south Africa, north and south America are water controlled. The most water-controlled sites are located in north Asia and South Africa. There is no detectable difference between northern and southern hemisphere.

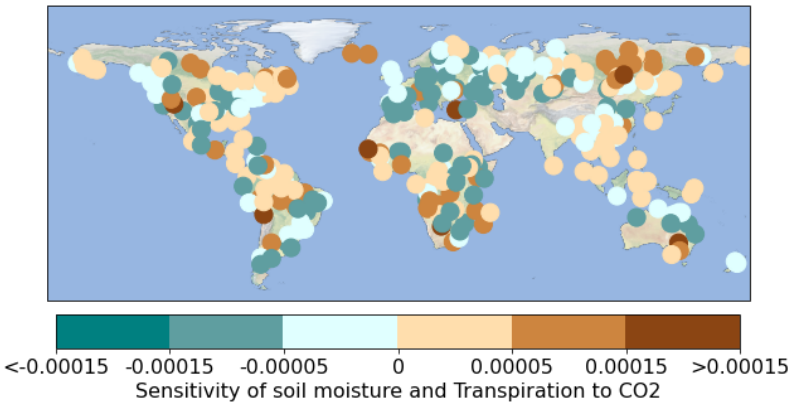

Figure 22. Global map for the Sensitivity of Δcor (sm',Tr_norm') to CO_2.

The water availability component of Δ ELI is shown in Fig. 22. Asia, north America, north of south America are mostly positive correlated while Europe, parts of south America and south Africa are mostly negative correlated. This correlation has the highest influence on the sensitivity of Δ ELI to CO_2 (cf. Fig. 21)

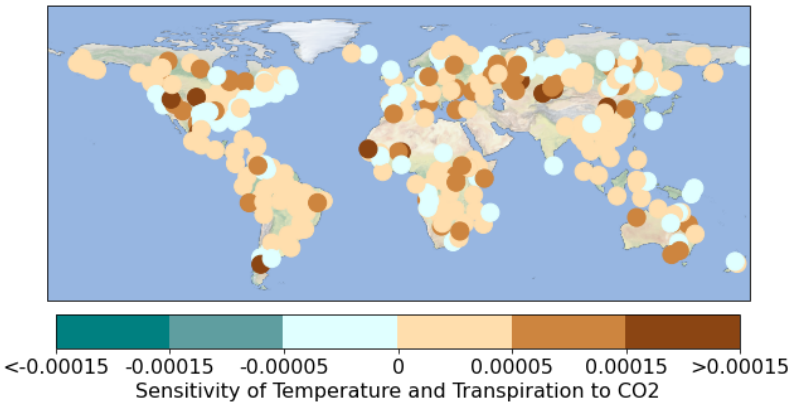

Figure 23. global map for the Sensitivity of Δcor (sm',Tr_norm') to CO_2.

The water availability component of Δ ELI is mostly positive. Only some regions in the northern hemisphere slightly water controlled (Fig. 23).

The following analysis the effect of Temperature, aridity, canopy height and LAI and the different PFTs for the sensitivity of Δ ELI to CO_2 are distinguished. TrBR is excluded in this analysis because the PFT is only represented with two sites in this study and therefore no regression is possible.

Table 3. Results from Multilinear Regressions.
P-values in brackets, PFTs in the first column, T = Temperature [K], LAI = leaf area index

	TrBE	TeBE	TeBS	BNE	BNS	TeH	TrH
R^2	0.336	0.589	0.387	0.052	0.875	0.204	0.027
T	0.7719 (0)	-0.261 (0.828)	-0.2824 (0.515)	0.3282 (0.193)	0.462 (0.452)	-0.0002 (0.019)	-8.3e-06 (0.899)
LAI	**-2,4284** (0.005)	**0.9096** (0.805)	-0.5892 (0.249)	**-0.3821** (0.128)	-0.118 (0.667)	-2.7e-05 (0.841)	-6.9e-06 (0.950)
canopy height	2.1839 (0.009)	-0.6129 (0.895)	**0.6076** (0.049)	0.0938 (0.734)	-0.5622 (0.263)		
aridity	-0.3278 (0.11)	-0.4141 (0,674)	0.1210 (0.577)	0.0865 (0.615)	**-0.7215** (0.386)	**-0.0003** (0.010)	**-0.0001** (0.270)

Tab. 3 shows the result from the Multilinear Regressions for each PFT. The first column represents the different PFTs. The first row shows the variables which influence on Δ ELI we want to test. The highest R^2 for the correlation is seen for BNS. This mean that the results for this calculation are closest to reality (cf. 2.4.3). The main driver for changes for the Sensitivity of Δ ELI are different for different vegetation types and PFTs. There are some similar results for PFTs with forest vegetation and for grass vegetation. For all the sites with forest vegetation except for TeBS and BNS changes of the sensitivity of Δ ELI to CO_2 are mostly influences due to changes in LAI. Changes for TeBS are most influenced due to canopy height. Changes for BNS are most influenced due to changes in aridity. For the forest vegetation except for TeBE and BNS aridity have the smallest influence on changes for Δ ELI. TeBE is at least influenced by Temperature and BNS is least influenced by LAI. There are similar driver for grass vegetation. Changes of Δ ELI on Grass sites are most influenced by changes in the Aridity. A small impact on these changes has the LAI – that's the opposite from what we calculated with forest vegetation. The p-values for each variable are differently reliable e.g. for the TeBE we have high value and for TrBE the values are near to zero.

3.1.4 d) Attribution of ELI with changes in time

First, I look at the attributions at a timeline of 118 years for the sites (Fig. 4). And later quantify the effect of them for Δ ELI with partial correlations.

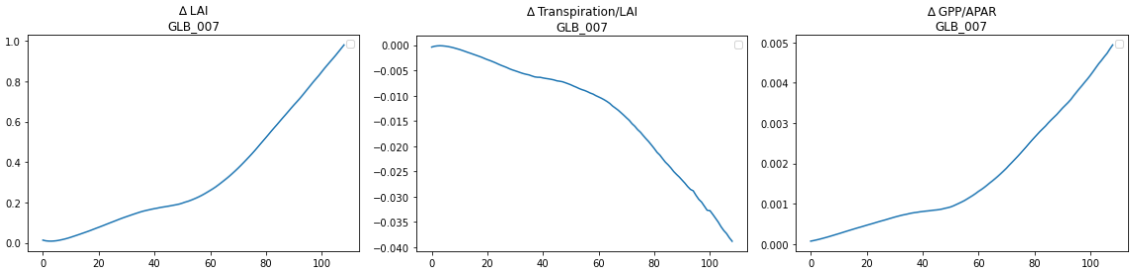

Figure 24. Attributions (Δ LAI, Δ Tr/LAI, Δ LUE) for the Tropical Forest.

We can see a weak increase of Δ LAI and Δ LUE for the first 50 years and then a stronger increase for the next couple of years. For Δ Tr/LAI we see a weak decrease for the first 50 years which change to a strong decrease for the last years in the Tropical Forest (Fig. 24).

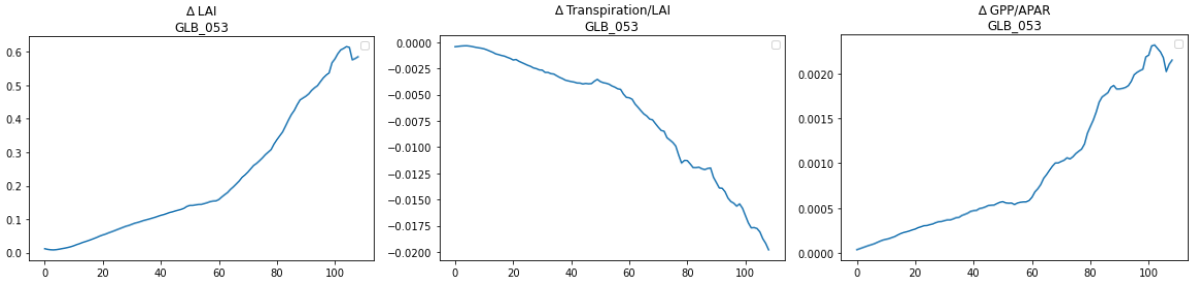

Figure 25. Attributions (ΔLAI, ΔTr/LAI, ΔLUE) for the Temperate Forest.

For the Temperate Forest we see the same effect of a weak increase in the first couple of years and then a stronger increase for the rest of the years for Δ LAI and Δ LUE. Δ Tr/LAI decrease during the years. We see more fluctuations for the values of the variables than for the variables for the Temperate Forest (Fig. 25).

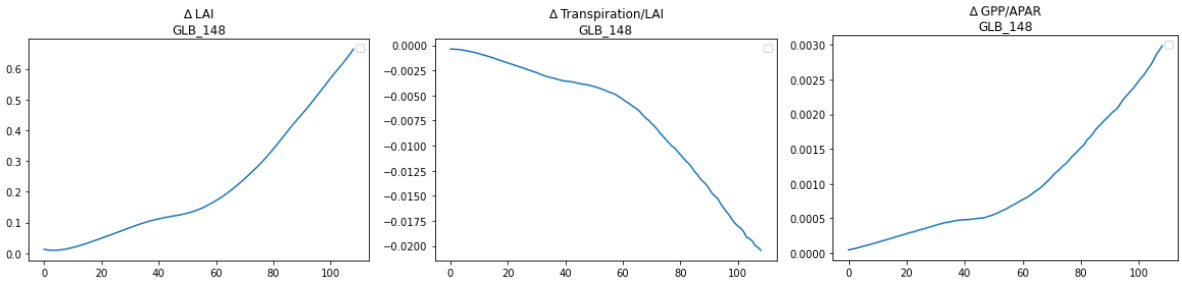

Figure 26. Attributions (Δ LAI, Δ Tr/LAI, Δ LUE) for the Boreal Forest.

The variables Δ LAI and Δ LUE increase while Δ Tr/LAI decrease over the years (Fig. 26).
To quantify the effect of changes in the attributions to changes in Δ ELI I plot in Fig. 24-26 I calculate the partial correlations.

Table 4. Results from Partial Correlation for three different sites.
P-values in brackets, LAI = leaf area index [m^{-2} m^{-2}], Tr = Transpiration [kg m^{-2} day^{-1}] GPP/APAR = light use efficiency

	Tropical Forest	Temperate Forest	Boreal Forest
Δ LAI	0.369 (0)	0.346 (0)	0.176 (0.07)
Δ Tr/LAI	0.494 (0)	0.104 (0.285)	0.243 (0.012)
Δ GPP/APAR	0.131 (0.179)	-0.262 (0.007)	0.155 (0.11)

The results for the partial correlations are summarized in Tab. 4. The first column shows the three selected sites we test (Fig. 4). The first row shows the values I choose to represent attributions. For the Tropical Forest and the Boreal Forest Δ Tr/LAI is most correlated with Δ ELI. This means Δ ELI is most influenced by the physiological effect of ΔTr/LAI for both sites.
The Temperate Forest site is most influenced by Δ LAI. This means that changes in Δ ELI can mainly be explained by structural changes from Δ LAI.

4 Discussion

In this section the result of the four analyses are discussed and compared to other findings.
In study a) the effect of increasing CO_2 on the limitation of energy and water for the vegetation is first discussed on a site scale. The Temperate, Boreal and Tropical Forest get more energy-controlled over the years with increasing CO_2 (Δ ELI, Fig. 7-9). The sites are located in south and North America and Australia. For this sites energy get more limiting with increasing CO_2 therefore precipitation has a lower influence for the sites compared to dry periods for the vegetation (cf. 1.1). With increasing CO_2, the plants absorb the same amount of CO_2 needed for photosynthesis through their stomata in a shorter time such that they lose less water vapour to the environment in this shorter time. This results in more photosynthesis with less water loss and therefore a higher WUE which leads to less water limitation or in other words more energy control (cf. 1.3).
Now we analyse the effect of increasing CO_2 not for all years as in the previous study. The global maps are only considering the month with the highest Transpiration. Here vegetation is most active. This is also shown in the map for the month with the highest Transpiration (Fig. 10). The northern hemisphere has the highest Transpiration in the summer months where photosynthesis is the highest while in the southern hemisphere the "winter" (summer in the southern hemisphere) months has the highest Transpiration (Fig. 10). The regime gets less energy limited when calculate the ELI for the month with the highest Transpiration than calculated for all years because of the high atmospheric water demand causes the high Transpiration which is associated with higher Temperature and therefore T is no longer limiting (cf. 2.4.1). Δ ELI

shows that high latitude sites in the northern hemisphere are getting less energy controlled because of an increase of the LUE due to increasing CO_2 (Fig. 12).
In analysis b) different components are used to compute the ELI. The results are later detailly compared with another study of Denissen et al., [2022b]
Analysis c) describe physiological and structural changes for changes in time for Δ ELI with Multilinear Regression (Tab. 3). For most sites with forest vegetation changes of the sensitivity of Δ ELI to CO_2 are mostly influences due to changes in LAI. This can be explained due the effect of increasing CO_2 for the CO_2 fertalization effect which leads to changes in GPP resulting in an increasing biomass production which influence changes in Δ ELI the most in most of the forest vegetation types (cf. 1.3). Changes of Δ ELI on Grass sites are most influenced by changes in the Aridity. The trend towards energy-controlled regimes is determined due the level of dryness in grasslands. This could be because trees generally have deeper rooting system than grass and can therefore access more soil moisture, so other factors affecting ΔELI more for the forest types [Aiba, 2016].
In analysis d) the changes of attributions in space for changes of the Δ ELI are quantified. An increasing LUE is detected because the increasing CO_2 stimulates the carbon assimilation and reduce the stomatal conductance resulting in an increasing LUE. The LAI also increase because of the CO_2 fertalization effect. Transpiration over LAI decrease because of the reduces stomatal conductance (c.f. 1.3). Δ ELI is most influenced by the physiological effect of ΔTr/LAI – the reduced stomata conductance with increasing CO_2 for the Tropical and Boreal Forest. In the Temperate Forest changes in Δ ELI can mainly be explained by structural changes from Δ LAI. The amount of leaves (quantified through Δ LAI) influences if the region is water or energy controlled.

In the following I will compare the results of my study with the results of another study from Denissen et al. [2022b] who established the ELI.

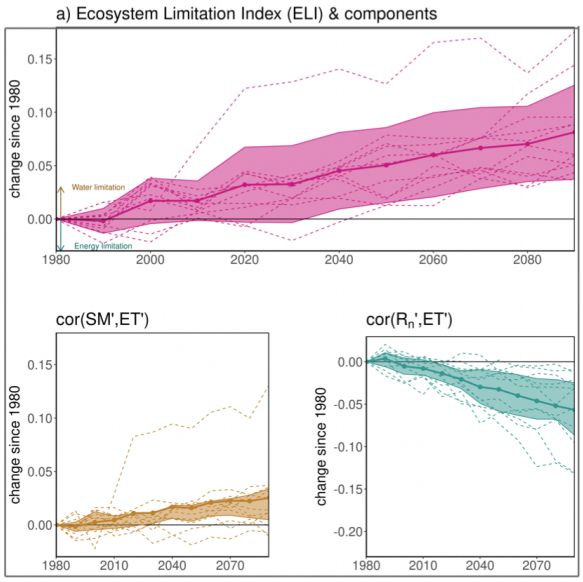

Figure 27. ELI and its components for the time scale from 1980 to 2080 [Denissen et al., 2022b].

Denissen et al., [2022] found a global continuous increase in ELI (more water control) over 73% of the warm land area throughout 1980–2100. Mainly reflected due to a decreasing correlation between terrestrial evaporation anomalies (ET') and surface net radiation anomalies (R_n') but also the increasing correlation with soil moisture anomalies (SM') plays a role [Denissen et al., 2022b].

The results in this study are different. With increasing CO_2 the ELI gets more energy controlled (Fig. 13, 21). This study verifies our hypothesis that the vegetation gets less water controlled at leaf level with increasing CO_2. Possible causes for the differences in ecosystem shift direction changes are discussed below.

In analysis b) I detect differences when I replace ELI with ELI_{Tr} or ELI_{ET}. Therefore, clear differences for the result of ELI are detected when calculated with different variables especially for ELI calculated with ET. In the here discussed study by Denissen et al., [2022b] ET' is used to compute the ELI. Different results can therefore be explained due to the use of different variables for ELI. Denissen et al. [2022b] also calculated the ELI with Tr' because this variable will increase in the future. Therefore, transpiration will have an increasing influence of vegetation for the land water and energy balances. They found out that when only Tr' for ELI is considered a similar but slightly weaker signal towards water limitation was found. Due the use of Tr' instead of ET' they also don't find a strong shift to water limitation [Denissen et al., 2022b].

Another difference is further the use of different time baselines in the studies. Denissen et al., [2022b] use data from 1980 until 2100 and therefore also make predictions for the future. In

my study data starting earlier (from 1900) lasting only until 2018 are used therefore the future is excluded. So, differences in results between both studies could be explained using different time periods. The shift towards water control in Denissen et al., [2022b] study could be explained due the further intensifying global warming in the future. This will lead to rising Temperature; therefore, Temperature is no longer limiting which leads to the decreasing Temperature correlation. Further this will lead to an increase in atmospheric water demand resulting in an increasing soil moisture correlation [Denissen et al., 2022b]. As in Tab.1 clarified these trends of the components lead to a positive ELI (water-control).

Another discrepancy for this study is different method of using Temperature or Radiation as energy variables. Mainly Radiation was used throughout the study of Denissen et al. [2022b]. They use the same energy variable throughout the calculations to compute the ELI. For the calculation in this study the energy variable of ELI was determined by computing Correlation between sm' with T' and sm' with SWR' an select the higher correlation for calculations (cf. Fig. 5). Denissen et al., [2022b] found out that while energy limitation for ELI calculated with Radiation and ELI calculated with T' are very similar, water limitation is stronger for the ELI calculated with radiation. The use of T' in water limited regions could result in a less water limitation and therefore a more energy limited regime.

Further differences results could be calculated due to the use of different models. In our study QUINCY is used (cf. 2.1). Denissen et al., [2022b] use CMIP6 data where 11 models are included. Which leads us to the limitation of this study.

5 Limitations

Models are an approximation to reality so the use of different models could lead to differences. As well as uncertainties for different parameter in the model could lead to different results.

This study is based on the ELI which distinguish between water- and energy limited regimes. This index is quite new and comparative literature and other studies that use this index are not yet available. The results of this study are compared and discussed only in relation to the results of Denissen et al., [2022a, 2022b].

Both simulation with the different CO_2 level used for this study are the simulations created in the study of Zhan et al. [2022]. The constant CO_2 level remain of the level of 296,8 ppm in 1901. The transient CO_2 assumes an increase of 110.63 ppm by the year 2018. There are discrepancies from reports e.g, published by government agencies or international organizations [Macknick, 2011]. According to UBA [2022] the CO_2 level in 1990 remain at 354,29 ppm with an increase of 53,83 ppm until 2018.

There are also uncertainties how increasing CO_2 affects the carbon and water cycle. Results of this effect from experiments and observations remain inconsistent [Zhan et al., 2022]. While results for WUE shows a strong increase for some studies [e.g., Keenan et al., 2013], in another studies [e.g., Knauer et al. 2017] WUE response less on increasing CO_2. There are also uncertainties how an increased WUE respond to changes in biomass. Some studies do not prove that an increased WUE leads to an increased tree biomass [e.g., Van der Sleen et al., 2015].
For this study confounding factors like nitrogen deposition and land cover change that potentially could influence the result were excluded when both simulations were calculated.
The reliability of study c) d) are shown due to p-values and R^2 (cf. Table 3 and 4). These values are close to zero for some calculations. The low R^2 tells that not much of the variation in the response is explained by the model therefore the low R^2 the model fits the data only limited [Akossou & Palm, 2013].
Study b) where different variables are used to compute the ELI could also be applied on a global scale to see the overviewing effect of the different variables. Now we only look at the site scale which could distort our findings.
To attribute changes of ELI with the time we calculate Partial correlations. One parameter we use to quantify physiological changes is ΔTr/LAI. Tr/LAI is also used to compute the ELI. In following studies another parameter should be used instead. So the correlation between Δ ELI and the parameter shows the real physiological change for changes in Δ ELI. Another parameter I can think of using is water use efficiency (WUE) reflected by $\mathrm{GPP} \times \sqrt{\mathrm{VPD}} / \mathrm{Tr}$ to be fair with the LUE – the other parameter we use to detect physiological changes. As an outlook for an additional analysis to understand physiological and structural changes for changes in Δ ELI global maps could be created to get an overview of the spatial pattern of the individual parameters and see how results change when using WUE instead of Δ Tr/LAI.

6 Conclusion

This thesis includes four analyses (a) studying the exclusive effect of CO_2 on ecosystem energy- vs. water limitation, (b) contrasting the energy- vs. water-limitation of different ecosystem variables Tr', norm_Tr' and ET', (c) understanding drivers of CO_2-induced changes in energy-vs. water-limitation (ELI) in time with considering physiological vs. structural vegetation changes, (d) understanding drivers of CO_2-induced changes in energy-vs. water-limitation (ELI) in space with considering climate and vegetation characteristics.

In summary, the thesis contains the following findings:

a) With increasing CO_2, the regime gets more energy controlled or in other words less water controlled at leaf level. Mainly reflected due to a decreasing correlation between transpiration anomalies and soil moisture anomalies but also the increasing correlation with Temperature or shortwave radiation anomalies.
b) There are differences of using different variables to compute the ELI. For the Boreal Forest the result gets more water controlled when using Tr_norm' or Tr' while there is a weaker signal towards an water-controlled regime with increasing CO_2 when using ET'.
c) For the sensitivity of Δ ELI to CO_2, the correlation of sm' and norm_Tr' has the highest influence. For most sites with forest vegetation changes of the sensitivity of Δ ELI to CO_2 are mostly influences due to changes in LAI. Changes of Δ ELI on Grass sites are most influenced by changes in the Aridity. A small impact on the changes for the Grass sits has the LAI – that's the opposite from what we calculated with forest vegetation.
d) Δ ELI is most influenced by the physiological effect of Δ Tr/LAI for the Tropical Forest and the Boreal Forest. Changes in Δ ELI can mainly be explained by structural changes from Δ LAI for the Temperate Forest.

7 Literature

Aiba, S. I. (2016). Vegetation zonation and conifer dominance along latitudinal and altitudinal gradients in humid regions of the western Pacific. In *Structure and function of mountain ecosystems in Japan* (pp. 89-114). Springer, Tokyo.

Ainsworth, E. A., & Long, S. P. (2005). What have we learned from 15 years of free-air CO_2 enrichment (FACE)? A meta-analytic review of the responses of photosynthesis, canopy properties and plant production to rising CO_2. *New phytologist*, *165*(2), 351-372.

Ainsworth, E. A., & Rogers, A. (2007). The response of photosynthesis and stomatal conductance to rising [CO_2]: mechanisms and environmental interactions. *Plant, cell & environment*, *30*(3), 258-270.

Akossou, A. Y. J., & Palm, R. (2013). Impact of data structure on the estimators R-square and adjusted R-square in linear regression. *Int. J. Math. Comput*, *20*(3), 84-93.

Anav, A., Friedlingstein, P., Beer, C., Ciais, P., Harper, A., Jones, C., Murray-Tortarolo, G., Papale, D., Parazoo, N., Peylin, P., Piao, S., Sitch, S., Viovy, N., Wiltshire, A., Zhao, M. (2015). Spatio-temporal patterns of terrestrial gross primary production: A review. *Reviews of Geophysics*, *53*(3), 785-818.

Blyth, E., & Harding, R. J. (2011). Methods to separate observed global evapotranspiration into the interception, transpiration and soil surface evaporation components. *Hydrological Processes*, *25*(26), 4063-4068.

Cao, X., Lin, D., Cai, L., Jiang, Y., & Zhu, D. (2017). Effects of different vegetation communities on soil carbon fraction, RubisCO activity and cbbl genes in Nanjishan wetland of Poyang Lake. *Acta Pedologica Sinica*, *54*(5), 1269-1279.

De La Fuente, A., Bing, N., Hoeschele, I., & Mendes, P. (2004). Discovery of meaningful associations in genomic data using partial correlation coefficients. *Bioinformatics*, *20*(18), 3565-3574.

Denissen, J. (2022a). *Mapping terrestrial evaporation regimes: a data-driven analysis of land-atmosphere interactions under climate change* (Doctoral dissertation, Wageningen University).

Denissen, J., Teuling, A. J., Pitman, A. J., Koirala, S., Migliavacca, M., Li, W., Reichstein, M., Winkler, A., Zhan, C., Orth, R. (2022b). Widespread shift from ecosystem energy to water limitation with climate change. *Nature Climate Change*, *12*(7), 677-684.

Dogutan, D. K., & Nocera, D. G. (2019). Artificial photosynthesis at efficiencies greatly exceeding that of natural photosynthesis. *Accounts of Chemical Research*, *52*(11), 3143-3148.

Duckworth, J. C., Kent, M., & Ramsay, P. M. (2000). Plant functional types: an alternative to taxonomic plant community description in biogeography?. *Progress in Physical Geography*, *24*(4), 515-542.

Fang, H., Baret, F., Plummer, S., & Schaepman-Strub, G. (2019). An overview of global leaf area index (LAI): Methods, products, validation, and applications. *Reviews of Geophysics*, *57*(3), 739-799.

Hauke, J., & Kossowski, T. (2011). Comparison of values of Pearson's and Spearman's correlation coefficients on the same sets of data. *Quaestiones geographicae*, *30*(2), 87.

Hauser, M., Orth, R., & Seneviratne, S. I. (2016). Role of soil moisture versus recent climate change for the 2010 heat wave in western Russia. *Geophysical Research Letters*, *43*(6), 2819-2826.

Hughes, L. (2000). Biological consequences of global warming: is the signal already apparent?. *Trends in ecology & evolution*, *15*(2), 56-61.

Joiner, J., Yoshida, Y., Zhang, Y., Duveiller, G., Jung, M., Lyapustin, A., Wang, Y., Tucker, C. J. (2018). Estimation of terrestrial global gross primary production (GPP) with satellite data-driven models and eddy covariance flux data. *Remote Sensing*, *10*(9), 1346.

Keenan, T. F., Hollinger, D. Y., Bohrer, G., Dragoni, D., Munger, J. W., Schmid, H. P., & Richardson, A. D. (2013). Increase in forest water-use efficiency as atmospheric carbon dioxide concentrations rise. *Nature*, *499*(7458), 324-327.

Klassen, S., & Bugbee, B. (2005). Shortwave radiation. *Micrometeorology in agricultural systems*, *47*, 43-57.

Knauer, J., Zaehle, S., Reichstein, M., Medlyn, B. E., Forkel, M., Hagemann, S., & Werner, C. (2017). The response of ecosystem water-use efficiency to rising atmospheric CO 2 concentrations: Sensitivity and large-scale biogeochemical implications. *New Phytologist*, *213*(4), 1654-1666.

Kolby Smith, W., Reed, S. C., Cleveland, C. C., Ballantyne, A. P., Anderegg, W. R., Wieder, W. R., Liu, Y.Y., Running, S. W. (2016). Large divergence of satellite and Earth system model estimates of global terrestrial CO2 fertilization. *Nature climate change*, *6*(3), 306-310.

Konarska, J., Uddling, J., Holmer, B., Lutz, M., Lindberg, F., Pleijel, H., & Thorsson, S. (2016). Transpiration of urban trees and its cooling effect in a high latitude city. *International journal of biometeorology*, *60*(1), 159-172.

Kumar, S., Zwiers, F., Dirmeyer, P. A., Lawrence, D. M., Shrestha, R., & Werner, A. T. (2016). Terrestrial contribution to the heterogeneity in hydrological changes under global warming. *Water Resources Research*, *52*(4), 3127-3142.

Lawlor, D. W. (2002). Limitation to photosynthesis in water-stressed leaves: stomata vs. metabolism and the role of ATP. *Annals of botany*, *89*(7), 871-885.

Lemordant, L., Gentine, P., Swann, A. S., Cook, B. I., & Scheff, J. (2018). Critical impact of vegetation physiology on the continental hydrologic cycle in response to increasing CO_2. *Proceedings of the National Academy of Sciences*, *115*(16), 4093-4098.

Macknick, J. (2011). Energy and CO2 emission data uncertainties. *Carbon Management*, *2*(2), 189-205.

Medlyn, B. E., Barton, C. V. M., Broadmeadow, M. S. J., Ceulemans, R., De Angelis, P., Forstreuter, M., Freeman, M., Jackson, S. B., Kellomäki, S., Laitat, E., Rey, A., Roberntz, P., Sigurdsson, B. D., Strassemeyer, J., Wang, K., Curtis, P. S., Jarvis, P. G. (2001). Stomatal conductance of forest species after long-term exposure to elevated CO_2 concentration: a synthesis. *New Phytologist*, *149*(2), 247-264.

Miralles, D. G., De Jeu, R. A. M., Gash, J. H., Holmes, T. R. H., & Dolman, A. J. (2011). Magnitude and variability of land evaporation and its components at the global scale. *Hydrology and Earth System Sciences*, *15*(3), 967-981.

Norby, R. J., & Luo, Y. (2004). Evaluating ecosystem responses to rising atmospheric CO2 and global warming in a multi-factor world. *New phytologist*, *162*(2), 281-293.

Ochsner, T. E., Cosh, M. H., Cuenca, R. H., Dorigo, W. A., Draper, C. S., Hagimoto, Y., Kerr, Y. H., Larson, K. M., Njoku, E. G., Small, E. G., Zreda, M. (2013). State of the art in large-scale soil moisture monitoring. *Soil Science Society of America Journal*, *77*(6), 1888-1919.

Pieruschka, R., Huber, G., & Berry, J. A. (2010). Control of transpiration by radiation. *Proceedings of the National Academy of Sciences*, *107*(30), 13372-13377.

Porporato, A., Laio, F., Ridolfi, L., & Rodriguez-Iturbe, I. (2001). Plants in water-controlled ecosystems: active role in hydrologic processes and response to water stress: III. Vegetation water stress. *Advances in water resources*, *24*(7), 725-744.

Prenger, J. J., & Ling, P. P. (2001). Greenhouse condensation control understanding and using vapor pressure deficit (VPD).

Sage, R. F., Way, D. A., & Kubien, D. S. (2008). Rubisco, Rubisco activase, and global climate change. *Journal of experimental botany*, *59*(7), 1581-1595.

Shakeel, A. A., Xiao-yu, X., Long-chang, W., Muhammad, F. S., Chen, M., & Wang, L. (2011). Morphological, physiological and biochemical responses of plants to drought stress. *African journal of agricultural research*, *6*(9), 2026-2032.

Sheugh, L., & Alizadeh, S. H. (2015, April). A note on pearson correlation coefficient as a metric of similarity in recommender system. In *2015 AI & Robotics (IRANOPEN)* (pp. 1-6). IEEE.

Su, Y., Gao, X., Li, X., & Tao, D. (2012). Multivariate multilinear regression. *IEEE Transactions on Systems, Man, and Cybernetics, Part B (Cybernetics)*, *42*(6), 1560-1573.

Tang, Y., Wen, X., Sun, X., & Wang, H. (2014). Interannual variation of the Bowen ratio in a subtropical coniferous plantation in southeast China, 2003-2012. *PLoS One*, *9*(2), e88267

Thum, T., Caldararu, S., Engel, J., Kern, M., Pallandt, M., Schnur, R., Yu, L., Zaehle, S. (2019). A new model of the coupled carbon, nitrogen, and phosphorus cycles in the terrestrial biosphere (QUINCY v1. 0; revision 1996). *Geoscientific Model Development*, *12*(11), 4781-4802.

Tommasi, I. C. (2021). The mechanism of Rubisco catalyzed carboxylation reaction: chemical aspects involving acid-base chemistry and functioning of the molecular machine. *Catalysts*, *11*(7), 813.

UBA 2022. https://www.umweltbundesamt.de/daten/klima/atmosphaerische-treibhausgas-konzentrationen, Stand 30.09.2022

Ueyama, M., Ichii, K., Kobayashi, H., Kumagai, T. O., Beringer, J., Merbold, L., Euskirchen, E. S., Hirano, T., Marchesini, L. B., Baldocchi, D., Saitoh, T. M., Mizoguchi, Y., Ono, K., Kim, J.,

Varlagin, A., Kang, M., Shimizu, T., Konsugi, Y., Bret-Harte, M. S., Machimura, T., Matsuura, Y., Ohta, T., Takagi, K., Takanashi, S., Yasuda, Y. (2020). Inferring CO_2 fertilization effect based on global monitoring land-atmosphere exchange with a theoretical model. *Environmental Research Letters*, *15*(8), 084009.

Ustin, S. L., & Gamon, J. A. (2010). Remote sensing of plant functional types. *New Phytologist*, *186*(4), 795-816.

Van Der Sleen, P., Groenendijk, P., Vlam, M., Anten, N. P., Boom, A., Bongers, F., Pons, T. L., Terburg, G., Zuidema, P. A. (2015). No growth stimulation of tropical trees by 150 years of CO_2 fertilization but water-use efficiency increased. *Nature geoscience*, *8*(1), 24-28.

Walker, A. P., De Kauwe, M. G., Bastos, A., Belmecheri, S., Georgiou, K., Keeling, R. F., ... & Zuidema, P. A. (2021). Integrating the evidence for a terrestrial carbon sink caused by increasing atmospheric CO_2. *New phytologist*, *229*(5), 2413-2445.

Wang, S., Zhang, Y., Ju, W., Chen, J. M., Ciais, P., Cescatti, A., ... & Peñuelas, J. (2020). Recent global decline of CO2 fertilization effects on vegetation photosynthesis. *Science*, *370*(6522), 1295-1300.

Way, D. A., Katul, G. G., Manzoni, S., & Vico, G. (2014). Increasing water use efficiency along the C3 to C4 evolutionary pathway: a stomatal optimization perspective. *Journal of Experimental Botany*, *65*(13), 3683-3693.

Wilhelm, C., & Selmar, D. (2011). Energy dissipation is an essential mechanism to sustain the viability of plants: the physiological limits of improved photosynthesis. *Journal of plant physiology*, *168*(2), 79-87.

Wullschleger, S. D., Tschaplinski, T. J., & Norby, R. J. (2002). Plant water relations at elevated CO_2–implications for water-limited environments. *Plant, Cell & Environment*, *25*(2), 319-331.

Yang, K., Ryu, Y., Dechant, B., Berry, J. A., Hwang, Y., Jiang, C., Kang, M., Kim, J., Kimm, H., Kornfeld, A., Yang, X. (2018). Sun-induced chlorophyll fluorescence is more strongly related to absorbed light than to photosynthesis at half-hourly resolution in a rice paddy. *Remote Sensing of Environment*, *216*, 658-673.

Zhan, C., Orth, R., Migliavacca, M., Zaehle, S., Reichstein, M., Engel, J., Rammig, A., Winkler, A. J. (2022). Emergence of the physiological effects of elevated CO_2 on land–atmosphere exchange of carbon and water. *Global Change Biology*.

Zhou, S., Williams, A. P., Lintner, B. R., Berg, A. M., Zhang, Y., Keenan, T. F., Cook, B. I., Hagemann, S., Seneviratne, S. I., Gentine, P. (2021). Soil moisture–atmosphere feedbacks mitigate declining water availability in drylands. *Nature Climate Change*, *11*(1), 38-44.